US HL-LHC ACCELERATOR UPGRADE PROJECT

# STRUCTURAL DESIGN CRITERIA

US-HILUMI-DOC-909

| |
|---|
| *Prepared by:*<br><br>Eric Anderssen, LBNL Project Engineer<br>Soren Prestemon, HL-LHC AUP Laboratory Representative, LBNL |
| *Reviewed by:*<br><br>Giorgio Ambrosio, US HL-LHC AUP MQXFA L2 Manager, FNAL<br>Thomas Page, US HL-LHC AUP Project Integration Engineer, FNAL |
| *Approved by:*<br><br>Ruben Carcagno, US HL-LHC AUP Project Manager deputy, FNAL<br>Giorgio Apollinari, US HL-LHC AUP Project Manager, FNAL |

## Revision History:

| Revision | Date | Section No. | Revision Description |
|---|---|---|---|
| v0.1 | 03/18/2018 | All | Draft for Comment |
| v0.2 | 03/29/2018 | All | General edits, and updated figures |
| v0.3 | 04/02/2018 | All | Initial Release for Review |
| v0.4 | 04/19/2018 | All | Release for Review |
| | | | |
| | | | |

# Contents

**Abstract**
This document provides design criteria for structural elements of the MQXFA high-field accelerator magnets, and specifically do not include the cryostat or helium containment vessel; these are adequately handled by the PED (Pressure Equipment Directive) and B&PVC (Boiler and Pressure Vessel Code). A graded approach is described which, when observed rigorously, is expected to yield structural designs that are safe for operation in the Large Hadron Collider. At each grade level criteria are defined which, if exceeded, will trigger the next level of analysis and/or require modifications to the design. Many elements of the document are taken directly from, or are based heavily on, relevant design criteria documents for other large magnet projects.

# 1 Introduction

The MQXFA series of superconducting quadrupole magnets (Main Quadrupole at Interaction region (X) series F, flavor A) will serve as focusing elements in the interaction regions of the Upgrade of the High-Luminosity Large Hadron Collider (HL-LHC). The purpose of this document is to provide guidance and guidelines for the design of the structural elements of the superconducting magnets.

The document first introduces the magnet components and provides a description of the primary load cases. We then review stress terminology (section 3) that will be used in the remaining sections of the document. Section 4 provides guidance on the analysis process that must be adhered to in evaluating the mechanical response of the system, and in particular identifies a graded approach to design evaluation. Finally in sections 5 and 6 the criteria for magnet component design are provided.

# 2 Component and Load Description

## 2.1 Magnet components

The mechanical structure for the MQXFA magnets has been developed specifically to address the brittle nature of the $Nb_3Sn$ superconducting material. In particular, coils, magnetic steel yokes, and a support structure provide prestress at room temperature, which is then increased during cool-down via differential contraction of the structural materials. The MQXFA cross section is provided in Fig. 1. The primary components and their associated material properties are provided in Table 1. Nominal values for key mechanical properties are provided in Appendix D, Table D.1. The values used in analysis must be conservative with respect to measured data on actual material.

| Component | Material | Standard |
|---|---|---|
| Axial rods | 316/316L | ASTM A479 13A |
| End plates | UNS S20910 (Nitronic 50) | ASTM-A-240-15 |
| Load pads (1) | ARMCO Grade 4 iron | EDMS 1744165 & 1802379 |
| Load pads (2) | 304CO | |
| Master keys | ARMCO Grade 4 iron | EDMS 1744165 & 1802379 |
| Shells | 7075 Aluminum | AMS 4126C, Grade 7075, T6 |
| Tie rods | 316/316L | ASTM A555/05, ASTM A580/08 (Chem) |
| Yokes | ARMCO Grade 4 iron | EDMS 1744165 & 1802379 |
| Collars | 6061 aluminum | |
| Master alignment key | Al Bronze C95400 | |
| Load key | 304SS | |

**Table 1:** Primary load-bearing materials used in the MQXFA magnet structure.

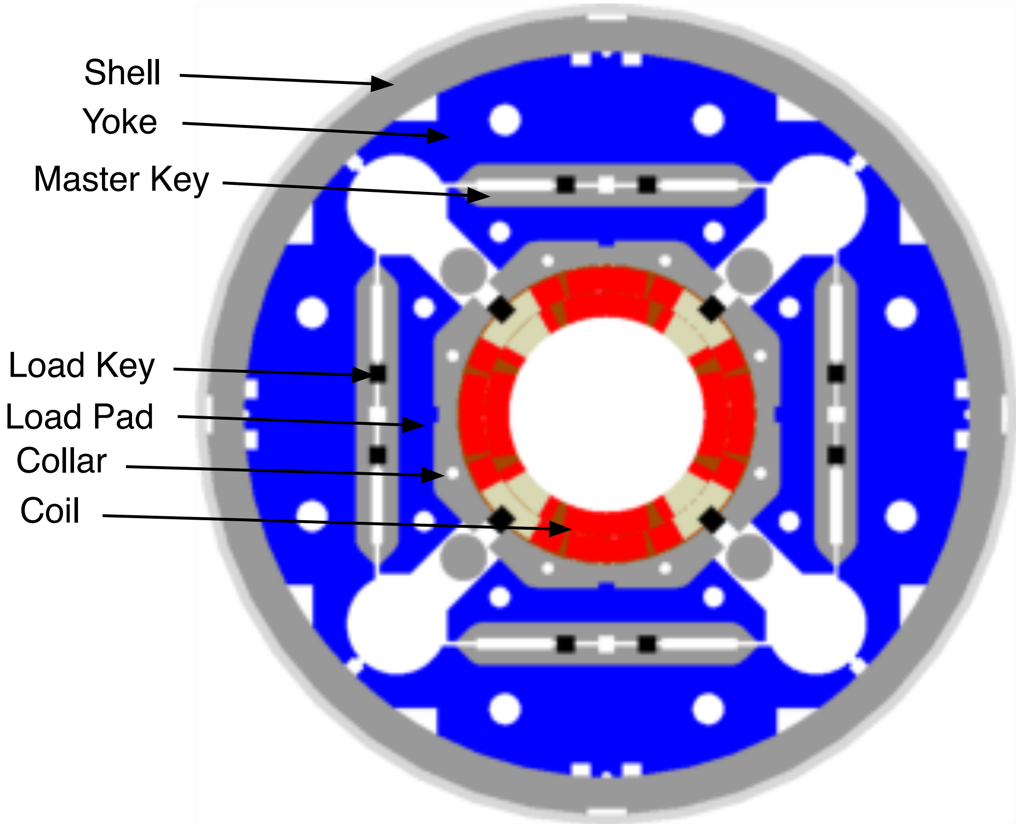


**Fig. 1:** Cross section of the MQXFA high-field superconducting magnet. The coil-pack assembly, composed of the coils and collars, are placed in a state of pre-compression via load keys, with the shell in tension providing the compressive force.

## 2.2 Load Terminology

To properly account for load scenarios in the application of design criteria, each component is evaluated under distinct loading condition that they are subjected to during their life cycle. For the MQXFA accelerator magnets, these are generally categorized as follows (see Table 2):

1. Assembly loading (1a) and room-temperature load (1b). The load(s) are typically associated with prestress operations that put the superconducting coils in a controlled state of azimuthal and axial compression. Note that stresses should be evaluated at all phases of the loading, since excursions beyond the loaded room temperature stress state may be encountered. Furthermore, due to constraints on the bladder pressurizing operation, the four-fold symmetry of the structure is broken, which can lead to variations in the stress distributions on components during that loading process.

2. Cool-down to cryogenic temperature, typically 4.2K or 1.8K. The resulting loading case includes the room-temperature loadings and thermal stresses induced by the differential thermal contraction of materials composing the structure.

3. Operation, i.e. the system is subjected to full Lorentz forces during normal operation; the loading includes the room temperature load (1a), the thermal induced loads associated with cooldown, and the forces associated with energization of the superconducting coils.

4. Fault Loads, i.e. loads outside of usual fabrication and operation. The fault scenarios to be considered may depend on the specific component under consideration; examples may include analysis

of eddy-currents in metal components induced by current extraction during quenching/fast extraction and the associated anomalous Lorentz forces, temperature-induced stresses emanating from a propagating quench, or stresses incurred during abnormal lifting or handling. In particular anomalous accelerations that can occur during shipment are of concern; typical values of acceleration are 3g. Note that in most handling scenarios coil strain considerations are the limiting consideration, rather than strength of materials criteria (see associated coil design criteria document ...).

| **Load case** | Loading (1a) | Loaded (1b) | Cooldown | Operation | Fault load |
|---|---|---|---|---|---|
| **Temperature** | 300K | 300K | 1.9K | 1.9K | Case-dependent |
| **Cycles** | $\sim 1-2$ | Static | $\sim 100$ | $\sim 5000$ | $\sim 1-2$ |

**Table 2:** Load case characteristics. The operational cycles is stipulated as a Functional Requirement in [17].

Since changes in load during operation (3) do not significantly change the stress states in the structural elements of MQXFA, and taking into consideration the low number of load cycles the magnets are subjected to (see Table 2), detailed fatigue analysis of structural components is not required. A summary of Functional Requirements for the MQXFA magnets is provided in [17].

## 3 Stress Terminology and Quantification

The terminology use in this document follows closely standard practice in mechanical analysis. Key elements are included here, largely taken from established design criteria documents for magnet systems ( [1], [2]), as well as relevant general design criteria formulations such as the ASME Fitness for Service ( [4]).

### 3.1 Stress Terminology

#### *3.1.1 Primary Stress*

These are stresses that could (if sufficiently high) contribute to plastic collapse, as distinct from secondary stresses, which do not. They can also contribute to failure by fracture, fatigue, creep or stress corrosion cracking (SCC). For the MQXFA quadrupoles the main concerns are plastic collapse and failure by fracture; creep, fatigue, and SCC are not considered. Primary stresses include all stresses arising from internal and external loads. For specific material component evaluation the primary stresses are divided into membrane ($\sigma_m$) and bending ($\sigma_b$) components as follows:

– Membrane stress, $\sigma_m$ is the average stress through the section thickness.

– Bending stress, $\sigma_b$ is the component of stress due to imposed loading that varies linearly across the section thickness.

The primary stress, ($\sigma_m + \sigma_b$), is simply the linear fit to the stress profile through the net section. The intercept of this linear fit with the component surface is the primary stress ($\sigma_m + \sigma_b$), shown in fig. 6 It is assumed here that the linear expansion starts at the locality of maximal stress. The intercept value is the primary stress and a primal assessment value used in this document.

Higher order polynomial approximations of the stress profile through the net section are useful for more advanced analyses such as fracture assessment. It should be noted that the terms in a higher order polynomial approximation are no longer equivalent to the primary stress, which is a simple linear fit.

### 3.1.2 Secondary Stress

Secondary stresses, sometimes referred to as residual stresses, are self equilibrating stresses that can generally be relieved by local yielding, heat treatment or other stress relief methods. They typically arise from fabrication processes such as welding, forging, forming or material removal processes in strain-hardening materials. They do not lead to plastic collapse of the net section since they are caused by localized strain limited phenomena, however they can contribute locally to the stress conditions at a crack tip in a flawed structure.

For the structural components of the MQXFA magnet structures made from heat-treated aluminum plate or forgings and iron, the post forming processes are not likely to induce significant secondary stresses, so are not considered in fracture analyses. Stainless steel components used in MQXFA are typically machined, leading to a small volume of material with residual stress on the surface machined– this zone on stainless steel components is usually much smaller than the critical flaw size for this material.

Secondary stresses are not considered for MQXFA structures. It should be noted that some design standards treat 'pre-load' stress in bolted joints as secondary stresses due to their strain limited nature. Here pre-loads are counted among the primary stresses in all cases.

### 3.1.3 Peak Stresses

Peak Stresses do not contribute to plastic collapse and are generally considered self-limiting, but must be considered against yield or fracture criteria as they generally exceed the primary stress and may dictate a higher grade of analysis to assure validity of subsequent failure criteria. Peak stress may be reported as either maximum principal (Section 3.2.1), or von Mises (Section 3.2.2) for various assessment critera.

Peak stresses generally occur at structural discontinuities under applied loads. For some geometries, such as sharp corners, the theoretical stress concentration factor is infinite. In these cases an elasto-plastic FEM analysis is required. Procedures defined in 4.3 are used to define the elastic limit at such locations, and report appropriate Primary and Peak stresses.

For MQXFA we expect peak stresses to emanate from stress concentration geometries. In all cases the concentrations can be evaluated using advanced FEA techniques (see section 4.3).

### 3.1.4 Yield and Ultimate Tensile stress

Yield Stress ($\sigma_y$) is the one-dimensional average stress at which a $0.2\%$ permanent strain offset is obtained, at the design temperature. Ultimate strength ($\sigma_u$) is the stress (based on the original area of the sample and at the design temperature T) at which the material fails. At $4$K, measurement of the value of $\sigma_u$ can be affected by serrated yielding where the temperature increase caused by plastic deformation results in lower or uncertain $\sigma_u$ values. $\sigma_y$ may also be affected but to a lesser extent. Different values may be obtained with different strain rates, and values can be affected by the sample cooling. Lowest reported values shall be used.

The stresses $\sigma_u$ and $\sigma_y$ are typically measured at room temperature, 77K (in liquid nitrogen), and 4.2K (in liquid helium) at atmospheric pressure. Intermediate values are difficult to obtain and are not generally available. The value of $\sigma_u$ referred to in these criteria is the maximum value obtained in a displacement controlled tensile test with a strain rate sufficiently low to minimize the effect of serrated yielding. The values at intermediate design temperatures will be determined by linear interpolation between these three temperatures, as this is generally recognized to be conservative.

### 3.1.5 Flow Stress

The Flow Stress ($\sigma_c$) is the stress required to sustain plastic deformation at a particular strain. It is the average (mid-point) value between $\sigma_y$, and $\sigma_u$.

$$\sigma_c = \left(\frac{\sigma_y + \sigma_u}{2}\right) \tag{3.1}$$

The Flow Stress is used in assessment of fatigue and/or fracture for assessment of crack propagation. At cryogenic temperatures, the ultimate tensile strength is sensitive to strain rates during the test, and the ratio of $\sigma_u$ to $\sigma_y$ is often decreased. Unless relevant data is available, $\sigma_c$ shall be replaced with $\sigma_y$ for the purpose of conservatism.

### *3.1.6 Fracture Toughness*

Fracture Toughness is typically evaluated using the plane strain fracture toughness or critical stress intensity factor $K_{Ic}$. Problems at cryogenic temperatures can occur due to the large specimen dimensions needed to obtain valid uniform crack growth fronts. The specimens can exceed the size of available test facilities or may not be obtainable from the size of component being used. In some cases special purpose tests must be developed to determine $K_{IC}$ by alternative routes, typically by using $J_{Ic}$ equivalence. For materials with significant plastic deformations the tests described in ASTM E399 [10] which is typically used to determine $K_{Ic}$ , are invalid or impractical. In this case using tests relying on the J-Integral, proportional to crack tip opening displacement (CTOD) can be used with the following equivalence:

$$K_{Ic} = \sqrt{\frac{EJ_{Ic}}{1-\nu^2}} \tag{3.2}$$

The critical stress intensity factor is a function of temperature. Depending on the material's crystaline structure, e.g. iron increases with temperature, some materials such as the aluminum used in MQXFA can slightly increase with decreasing temperature [15]. Use of a measured $4$K value in structural assessments is always conservative and is acceptable. Otherwise, linear interpolation must be used between data points at $4$K, $77$K and room temperature.

## 3.2 Stress Quantification

The stresses for use in the following assessment procedures are calculated for an un-flawed component. All analyses assume linear elastic behavior of the materials, with attention to areas of peak stress described in 3.1.3. In these regions the stress may vary non-linearly through the thickness of the component, in these cases the primary stress may be expanded to higher order terms beyond $(\sigma_m + \sigma_b)$ as described in 3.1.1 to account for the peak stress non-linearity. This is required for fracture calculations.

### *3.2.1 Principal Stress*

The maximum principal stress $\sigma_p$ is used for comparison to fast fracture criteria. It includes primary, secondary, and peak stresses. It is also used in fatigue analyses. If the maximum principal stress, or the von Mises stress (described in section 3.2.2) exceed the yield stress, an elasto-plastic analysis is required to establish $\sigma_p$ for use in fatigue or fracture calculations.

The principal stresses can be obtained by diagonalizing the stress tensor, sometimes called the Cauchy stress tensor, which reduces shear (off-diagonal) elements to $0$; for simplicity, these principal stresses are $\sigma_1, \sigma_2$, and $\sigma_3$ the maximum principal stress $\sigma_p$ is the maximal of these three principal stresses, plus any secondary stress, if deemed necessary for the analysis. These principal stresses, or the stress tensor can be readily extracted from FEM results described in section 4 which can include primary and peak stresses.

### *3.2.2 von Mises Stress*

The von Mises stress has been adopted for combining stress components for comparison to plastic failure criterion. The von Mises stress $\sigma_v$ is scalar in nature, sometimes called the equivalent stress, and is related to second tensor invariant of the deviatoric component of the Cauchy stress tensor, which is the component of stress remaining after subtraction of the hydrostatic component, i.e. when the principal stresses differ from each other. The deviatoric stresses contribute to distortion where the hydrostatic components contribute to contraction or dilation. The von Mises stress can be written directly from elements of the stress tensor.

$$\sigma_v^2 = \frac{1}{2}[(\sigma_{11} - \sigma_{22})^2 + (\sigma_{22} - \sigma_{33})^2 + (\sigma_{33} - \sigma_{11})^2 + 6(\sigma_{12}^2 + \sigma_{23}^2 + \sigma_{31}^2)] \tag{3.3}$$

Using the principal stresses defined in section 3.2.1, equation (3.3) can be simplified. The off-diagonal terms reduce to 0 and the on-diagonal terms reduce to the principal stresses, $\sigma_1$, $\sigma_2$, and $\sigma_3$.

For materials that do not respond to hydrostatic stresses, e.g. all metallic structural components in MQXFA, the von Mises stress is used to compare to the yield stress, $\sigma_y$ to predict onset of yielding. The von Mises (equivalent) stress is also used in assessing comparative stresses on composite magnet coils with appropriate material constants.

## 4 Analysis Procedures

A graded approach to mechanical analysis is assumed, shown in fig. 2, wherein the design criteria are evaluated using consecutively more advanced and detailed analysis as the component and load case are found to result in reduced margin with respect to relevant mechanical figures of merit. These are described in Section 5. Analysis results shall always report the Primary Stress ($\sigma_m + \sigma_b$), and the Peak Stress, either as $\sigma_p$, or as $\sigma_v$ depending on relevant criteria. As these are typically the result of Finite Element Analyses, described in this section, reports will contain the relevant assessment stress.

Failure can occur via a) plastic collapse, typically associated with "tough" materials that yield in a smooth manner under the influence of large loads, b) linear elastic fracture, typically associated with brittle materials under significant loads coupled with stress concentration factors such as defects or voids, or c) ductile tearing, i.e. materials subjected to a combination of the elements above. Using either critical stress intensity ($K_{Ic}$) or Yield or Flow stress solely can yield non-conservative designs, in particular in the range of 0.3-0.9 $\sigma_c$, or $\sigma_y$ . An approach that includes the full range of failure modes, such as described in the R6 [6], will be used. A schematic assessment showing these modes, known as the "Failure Assessment Diagram"(FAD) is shown in Fig. 3. It shows a transition region, 'Ductile Tearing' where neither flow stress, or stress intensity FoM dominate. How this is used will be described in section 5.

For all materials used in the MQXFA magnets, material certification is expected. For each component and loading condition the R6 diagram should be evaluated and the associated "load-line" determined to evaluate if the component is limited by fracture or by plastic collapse. The FAD is simply the formula:

$$K_r(S_r) = S_r \left[ \frac{8}{\pi^2} \log \left( \sec \left( \frac{\pi}{2} S_r \right) \right) \right]^{-1/2}. \tag{4.1}$$

and is obtained from measured $\sigma_y$, $\sigma_u$ and $K_{Ic}$ values to determine the unit range of the horizontal and vertical axes. The 'Load Point', $(S_r', K_r')$ parameters defined by $K_r' = K_I/K_{Ic}$ and $S_r' = 2\sigma_a/\sigma_c$.

Here $K_I$ is the Mode I stress intensity factor and $K_{Ic}$ is the critical stress intensity based on the Douglass-Barenblatt strip yield model [12], [13]. $S_r'$ is the stress at assessed load ($\sigma_a$) over the flow stress. Methods to use the FAD are described in Section 5.

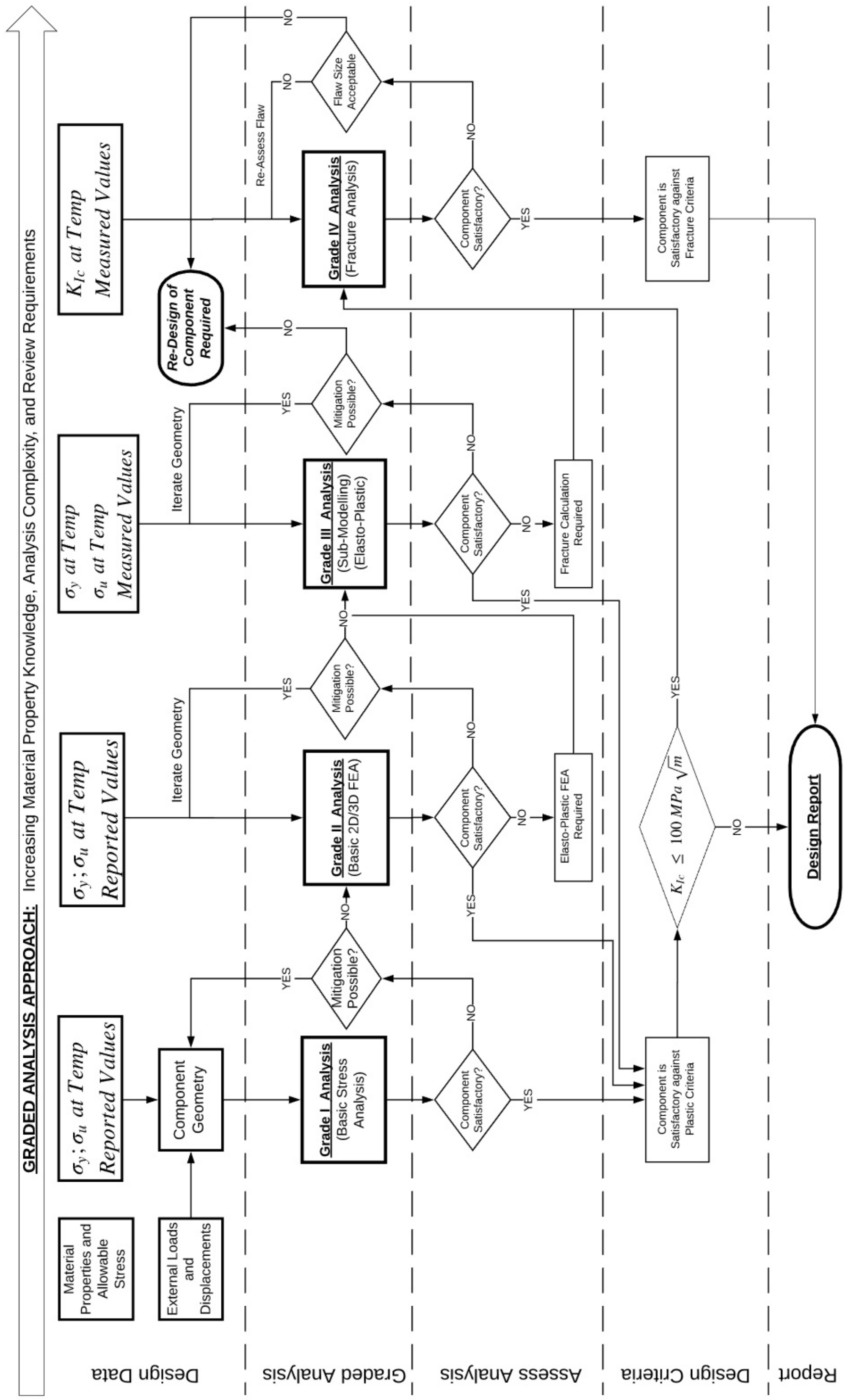


**Fig. 2:** Schematic of Graded Approach to Analysis Procedures. These are expanded in following sections.

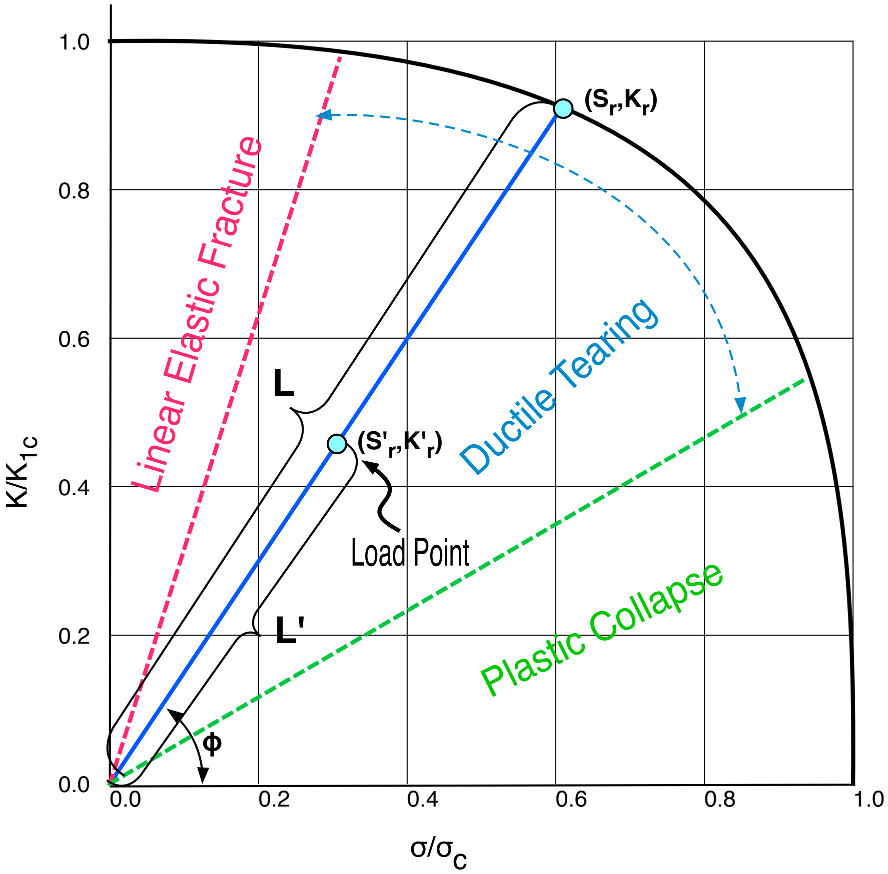


**Fig. 3:** Schematic description of the possible failure modes associated with magnet materials.

### 4.1 Grade I: Basic stress analysis

The stress analysis of the MQXFA Magnets and related components will be performed with analytical formulations evaluated by hand and/or computer codes. It is expected that a finite element analysis will be performed for most structural components. However for some elements, such as bolt sizing analytic formulations can be used. These will report only membrane stress or simple bi-axial stresses, e.g. in bolts, and tension members; where significant bending is expected in such members, Grade II analysis is required.

Well established guidelines must be adhered to in the application of analytic formulations. In particular appropriate boundary conditions must be applied and condition of validity for formulas must be satisfied. The source of all analytic equations, and material properties assumed in the analysis must be documented. Appendix D provides an overview of the material properties used for the primary metallic components of MQXFA.

As shown in fig. 4, mitigation steps during the analysis section may be allowed to stay within a Grade I analysis regime. These may include moderate changes to the geometry, such as increasing section, change of thread pitch, change of alloy to higher strength, or inclusion of simple stress reduction features such as fillets. In general, no fracture analysis will be based on a Grade I analysis. If standard mitigation efforts are ineffective, or the analysis shows a more complicated analysis is required, moving to a Grade II Analysis is required.

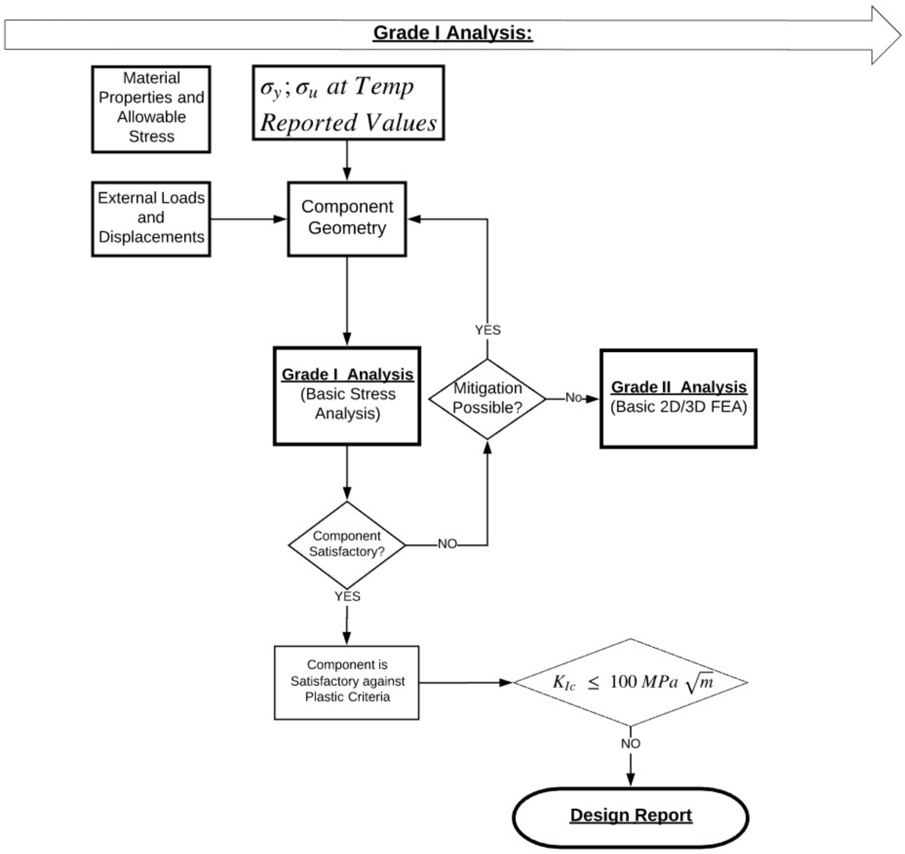


**Fig. 4:** Flowchart describing Grade I Stress Analysis procedure.

## 4.2 Grade II: Basic 2D and 3D FEA

Due to the complexity of the magnet design and the various load conditions encountered during fabrication, assembly, and operation, most structural elements of the MQXFA magnet are subjected to 2D and/or 3D FEA, as deemed appropriate by the design engineer. Standard FEA practice must be adhered to, with well-defined boundary conditions and clearly documented interface conditions. Material properties must be based on measured data taken at appropriate temperatures; if data is taken from the literature, references must be provided documenting the conditions under which the experiments were taken and the chemical composition of the material measured. These are generally available in Appendix D. Many components in the MQXFA magnet can stop with a report after a successful Grade II analysis is completed.

If the FEM analysis show stress concentrations, these must be addressed by grid refinement or utilizing techniques outlined in the next section (4.3). To confirm a Peak Stress, a minimum of two grid refinement steps showing no significant change in the calculated stress concentration must be performed. In general, this level of analysis will report Primary Stress and Peak Stress below the Yield Stress, if mesh refinement proves too analytically heavy to account for mitigation features, e.g. fillets, for a Grade II Analysis, the next grade of analysis employing sub-modeling is required.

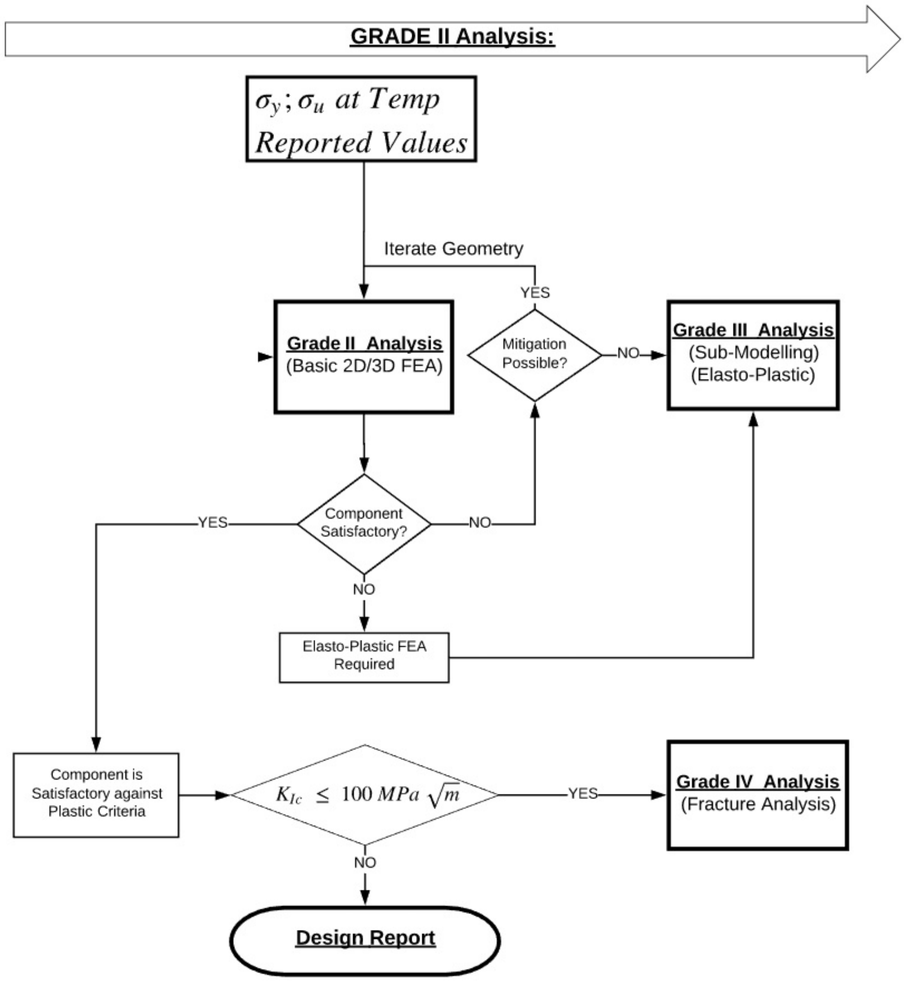


**Fig. 5:** Flowchart describing Grade II Stress Analysis procedure.

### 4.3 Grade III: Advanced FEA techniques

For components exhibiting stress concentrations that cannot be readily resolved via routine mesh refinement studies in the primary FEA model, sub-modeling can be performed to determine the stress concentration factor. A local region (area or volume) encompassing the stress concentration zone is identified and a FEA model of the region made; displacements from the original model are then imposed on the appropriate boundaries of the local region model (sub-scale model). Mesh refinement on the sub-model is performed until the stress concentration is fully resolved (i.e. convergence is obtained). The typical process flow and example grid is shown in Fig. 7. The sub-model boundary stresses must be compared with the original model stresses to verify that St. Venant's principle is valid for the sub-model, i.e. that the fully resolved stress concentrations in the sub-model are negligibly affecting the stress distribution in the original FEA model. A reasonable requirement is

$$\frac{||(\sigma_{ij} - \sigma_B) \cdot \vec{n}||}{||\sigma_{ij} \cdot \vec{n}||} << 1; \qquad ||\sigma_{ij} \cdot \vec{n}|| = \int_S ||\sigma_{ij} \cdot \vec{n}||^2 dS \tag{4.2}$$

where $S$ is the interface surface of the sub-model, $\sigma_{ij}$ is the calculated stress tensor after refinement, and $\sigma_B$ is the "Baseline" stress tensor from the original full model. Particular attention must be taken when sub-models are used in the vicinity of symmetry boundary conditions to verify that they are properly accounted for in the model and in the determination of validity of St. Venant's principle.

Note that under certain conditions linear elastic material behavior results in non-physical singularities. The local stress concentration will then result in local plastic deformations that limits the effective stress state. If the material is known to have elasto-plastic properties under the corresponding load and temperature conditions, these properties will be taken into consideration in the FEA model; under such conditions it is expected that thorough grid refinement studies are performed to verify that the resultant peak stress is reliably determined, and an elastic region is established.

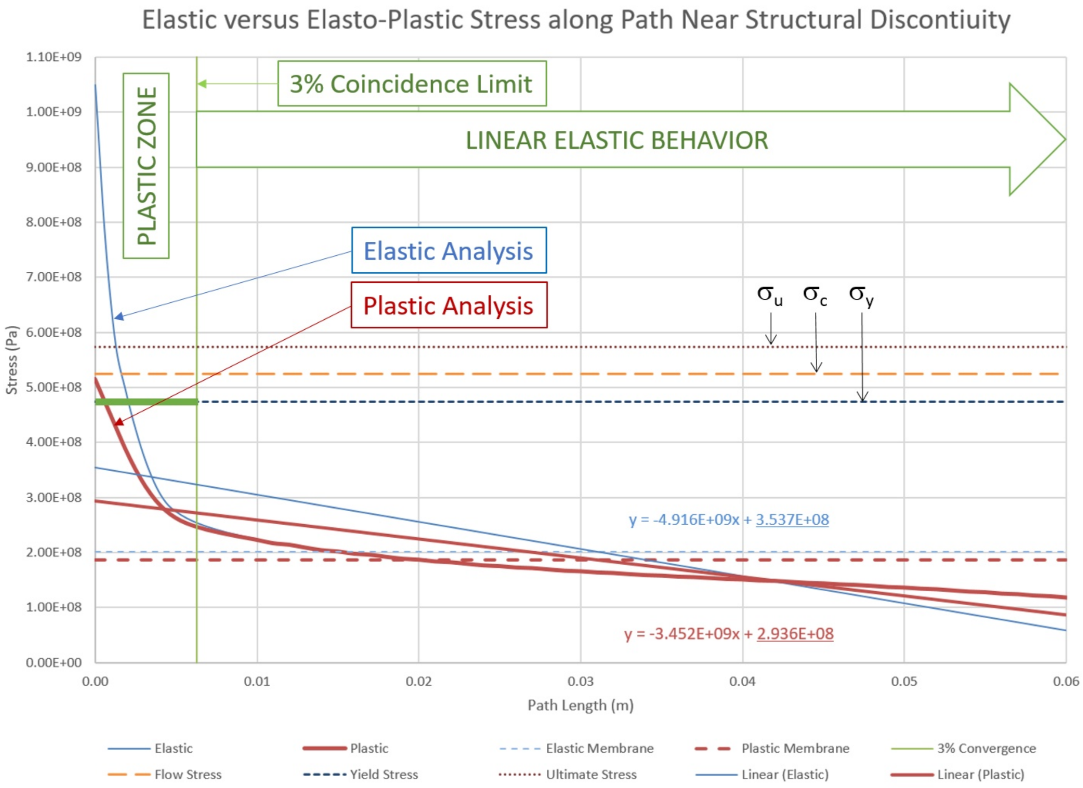


**Fig. 6:** Elastic FEM results versus Elasto-Plastic showing the Primary Stresses and estimate of Plastic Zone. Results shown for a 7075 Aluminum section 6 cm thick using a multi-linear yielding model.

It is shown in fig. 6 that the 'non-physical' fully elastic analysis will coincide with the elasto-plastic model at some distance from the structural discontinuity, in this example $\sim 6$ mm. A coincidence limit of 3% is chosen to limit the number of mesh refinements required in FEM. It is accepted that either the elastic or elasto-plastic model is predictive of local stress beyond this point. This method will be used to estimate the region of elastic behavior in Section 4.4. It can also be seen that the Primary Stress is lower for the Elasto-Plastic analysis. The underlined values in the linear estimate equations are the Stress intercepts at $x = 0$, in the plot and represent the Primary Stress ($\sigma_m + \sigma_b$) of each solution. The Elasto-Plastic Primary Stress is $\sim 20\%$ less than that predicted by the fully Elastic solution, however the Membrane Stresses deviate by $\sim 5\%$. Elasto-Plastic analysis is required in regions of structural discontinuity.

Where possible it is recommended to modify the design ('mitigation' in fig. 5), to either avoid stress concentrations resulting in plastic deformations, or limit the size of the plastic region for subsequent analyses. Examples include the introduction of fillets or radii to corners. Where Fracture is not a concern, it is still possible that the end result of a Grade III Analysis may require Re-design of the Component.

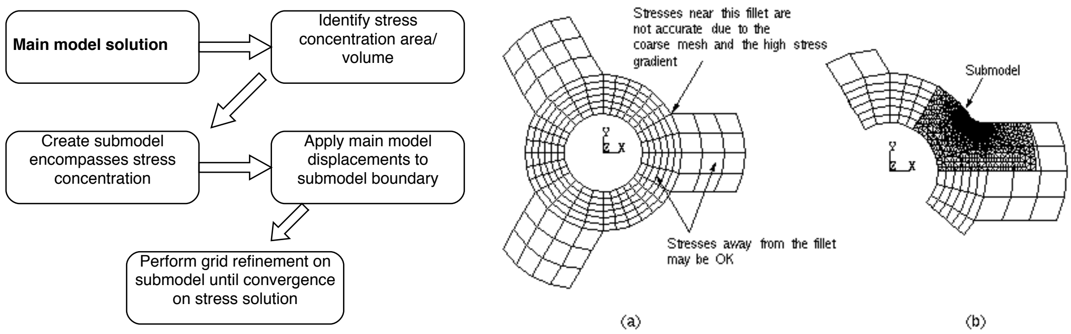


**Fig. 7:** Left: Flowchart of the basic process for subscale modeling; Right: example from ANSYS® of submodel region with fine mesh.

### 4.4 Grade IV: Stress Intensity Analysis

Many materials exhibit fracture failure modes at room and cryogenic temperature, and a systematic and sufficiently conservative approach must be taken to avoid material failure. The approach described here relies on the R6 design criteria approach [6], which has been adopted by ASME FFS-1, Fitness for Service standard [4], and adapted here to the specific needs of the MQXFA superconducting magnet structures. In all cases the stresses used to calculate the stress intensity will come from results of a previous grade of analysis, but likely Grade II or III.

For the purposes of design, semi-elliptic part-through cracks are assumed with flaw features intersecting and centered on the components surface as these typically have the highest stress intensities. A discussion of analysis approach, assumptions, and validity follows.

#### *4.4.1 Applied stress intensity $K_I$*

Linear Elastic Fracture Mechanics (LEFM) analysis methods apply to structures where crack tip plasticity is small. LEFM should not be applied to structures that exhibit significant plastic flow. For the purpose of this document, we will only use LEFM, and not take advantage of reserve strength available for significantly ductile materials such as stainless steels.

Only Mode I loading is assessed as Modes $II$, and $III$ typically are not seen in MQXFA structures, and have higher critical assessment values. The Mode I stress intensity factor can be expressed in the following form:

$$K_I = Y\sigma\sqrt{\pi a} \tag{4.3}$$

Where $Y$ is a dimensionless geometry factor, $\sigma$, is a characteristic stress, and $a$ is the characteristic flaw dimension. If the geometry factor is known, the stress intensity $K_I$ can be calculated for any combination of $\sigma$, and $a$. The applied stress intensity can then be compared to the relevant material property, here $K_{Ic}$. Many stress intensity solutions have been published and are available in handbooks [9], [4] and the appendices of many fracture mechanics texts such as Anderson [14].

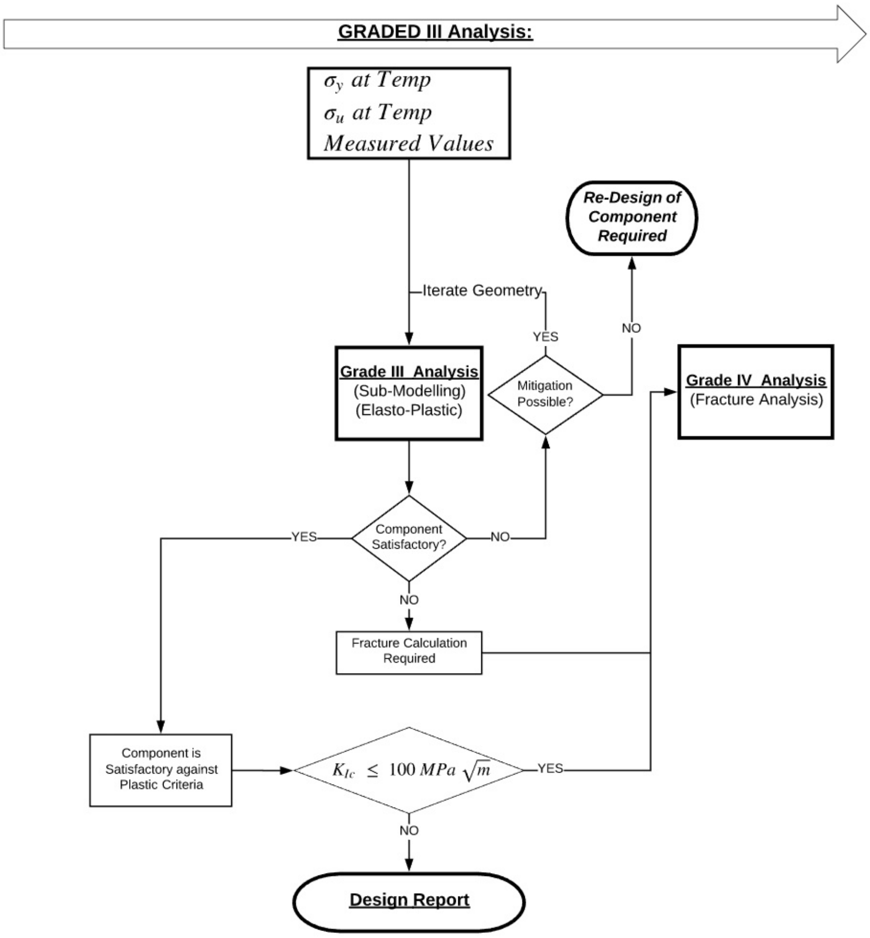


**Fig. 8:** Flowchart describing Grade III Stress Analysis procedure.

### 4.4.2 $K_I$ for Part-Through Cracks

Many solutions have been published for applied stress intensity based on linearized stresses that are decomposed to $\sigma_m + \sigma_b$ the membrane and bending stresses described in section 3.1.1. These solutions for part-through cracks subject to primary stresses can be written in the following form:

$$K_I = (\sigma_m + H\sigma_b)\ F \sqrt{\frac{\pi a}{Q}} \tag{4.4}$$

Where

$$Q = 1 + 1.464\ (\frac{a}{c})^{1.65} \tag{4.5}$$

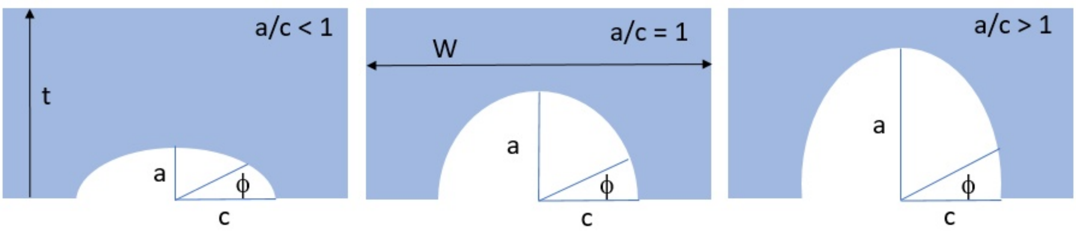


**Fig. 9:** Part-Through crack geometries with definitions of a, c, and $\phi$.

The flaw shape parameter $Q$ is a function of the ratio $a/c$, and is the the first two terms of a series expansion of the solution of an elliptical integral of the second kind. It is meant to account for finite crack geometry, and is used in most published literature [14]: Appendix 2. $F$ and $H$ are geometry constants that can be obtained from FEA or published data. This is a reasonable approximation for pressure vessels and other structures where the load profiles are predominantly linear, or linearized, but this can miss peak stresses that are often present near local structural discontinuities. Equation 4.4 is a special case of the *influence coefficient approach* described later in this section.

More generally, the normal stress $\sigma_{yy}(\mathrm{x})$ as illustrated in figure 10 can be approximated as a cubic expansion of a load profile extracted from an un-flawed elastic analysis in the direction of assumed crack propagation through part thickness $x = a$ direction.

$$\sigma_{yy}(x) \approx \sum_{i=0}^{3} A_i x^i \tag{4.6}$$

This approximation better captures more complex through thickness load profiles, and better approximates the peak stress, and should be applied as appropriate for MQXFA analysis. A detailed example extracted from an elastic ANSYS solution is shown in figure 11, which shows the discrepancies between peak stress, the approximation in equation 4.6, and the stress profile approximated by the primary stress across the component thickness. The data points for the stress extracted from ANSYS are shown as diamonds, with no curve through them.

For the indicated crack length of 10mm in figure 11, both the primary stress ($\sigma_m + \sigma_b$), and polynomial fit over-predict the local stress. For a crack of 5 mm, they are all very similar, but for cracks smaller than 5 mm, the stress at the crack tip is better approximated by the cubic fit. This fit can be

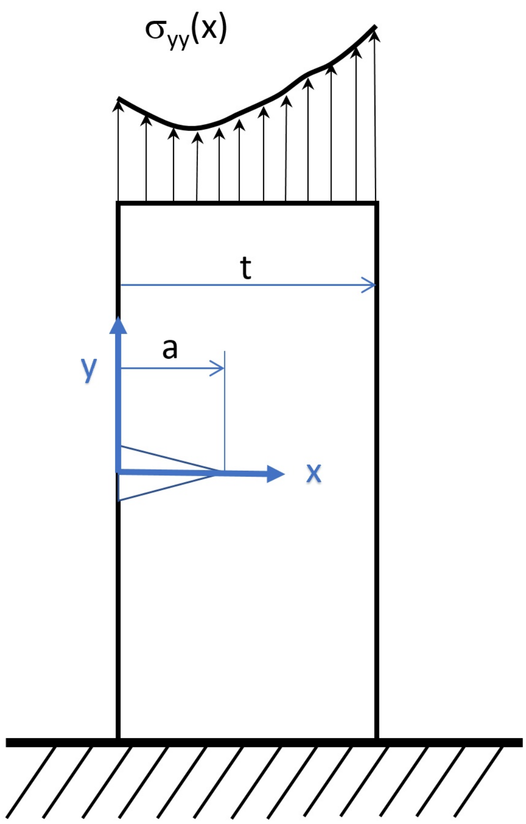


**Fig. 10:** Cantilever Beam with arbitrary load.

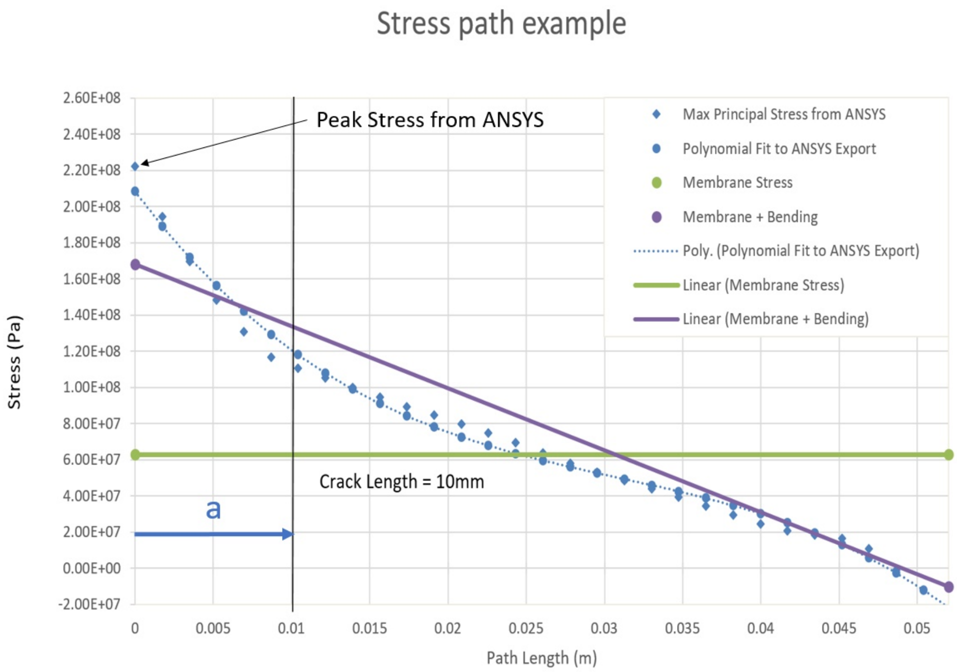


**Fig. 11:** Approximations of stress profile through part thickness using data extracted from ANSYS FEM; Membrane, and Membrane + Bending stresses are also reported by ANSYS

improved by only fitting the data from $0 \leq x \leq a$.

For the purposes of an initial assessment to determine a critical crack length, it is useful to first use the expansion through the entire component thickness then limit the expansion to the region near the critical flaw size. It is also important to assess how well the expansion follows the stress distribution by generating plots such as shown in figure 11.

The *influence coefficient approach* better approximates the stress at the crack tip. The stress intensity $K$ is proportional to $\sigma\sqrt{a}$, with some geometry modification factor $F$. The mode-I stress intensity can be written as:

$$K_I = F\sigma\sqrt{\frac{\pi a}{Q}} \tag{4.7}$$

Using Equation 4.6, $F\sigma$ can be approximated as

$$F\sigma(x) = \sum_{i=0}^{3} G_i A_i x^i \tag{4.8}$$

The $G_i = G(\frac{a}{c}, \frac{a}{t}\frac{t}{R_i}, \phi)$, known as 'influence coefficients,' are geometric factors that enhance $K_I$; see figure 9 for definitions of $a$, $c$, $\phi$, and $t$. $R_i$ is the radius of curvature near the crack surface. It is shown in Anderson [14], and appendix A.2 in this document, that the $G_i$ are not a strong function of $(t/R_i)$ so that a part through crack in a simple cantilever beam is a good approximation for moderately curved sections. For all components other than the thick walled cylindrical shell, this cantilever model shall be used in analyses. For the case of the shell, influence coefficients specific to cylindrical shells shall be used.

Expanding equation 4.7 with equation 4.8,

$$K_I = \sqrt{\frac{\pi a}{Q}}(G_0A_0 + G_1A_1a + G_2A_2a^2 + G_3A_3a^3)f_W \tag{4.9}$$

Where

$$f_W = \left[sec\left(\frac{\pi c}{2W}\sqrt{\frac{a}{t}}\right)\right]^{\frac{1}{2}} \tag{4.10}$$

The $A_i$ are from the expansion in equation 4.6, and the $G_i$ are available for typical geometries of MQXFA in Appendix A. For definitions of a, c, t, and W used in $f_W$ see figure 9, this is a shape parameter used to account for the finite width and thickness of the component, by convention, c is in the Width direction and a, is in the thickness dimension. The angle $\phi$ is 0 when aligned in the c direction and $\frac{\pi}{2}$ when aligned with the through thickness dimension (x) in figure 10. This approximation is used for all components that are not cylindrical shells, or round rods in tension.

### *4.4.3 Flaw Geometry used in Analysis*

For the purpose of design criteria where Grade IV analysis is required, a semi-elliptic surface flaw will be assumed at the location of peak stress with the least favorable opening orientation, i.e. normal to $\sigma_p$ (maximum principal stress). The flaw will be assessed as a circular thumb-nail crack with a geometry ratio of $a/c = 1$, with influence coefficients selected for the $\phi = 0$ $(c)$ direction, which are highest for this geometry. Discussion of validity of this assumption is available in Appendix A. This is a conservative approach, as crack propagation in the thickness $(a)$ direction $(\phi = \pi/2)$ is the primary concern. However, if a flaw of nominal size with this geometry does not propagate in the "$c$" direction, it shall not in other directions.

### *4.4.4 Assess Critical Flaw Size*

Assessed flaw size, $a$, will be increased in analysis to determine a 'critical' flaw size, where $K_I$ approaches a 'critical' characteristic assessment value e.g. $K_{Ic}$. This critical flaw size will be used to both determine inspection limits and rejection criteria for components. A discussion of this process is available in Appendix B. It is assumed that this analysis remains in a purely elastic region. This stipulation may require refinement of results from Grade II or III analyses to provide relevant elastic inputs for this assessment to remain valid.

During assessment of critical flaw size, a validity check on the use of the influence coefficient approach is required for the assumption of semi-elliptic flaw geometry. In the limit case with $a/c = 1$ and an infinitely wide section, the crack length '$a$' can approach, even exceed, the the through-part thickness '$t$' with solutions remaining valid for applicable $\phi$, however the crack width '$2c$' must never exceed $0.5W$ (component Width). When $2c$ approaches the component width $W$, the solution changes from a semi-elliptic crack to a full width crack. This condition is normally not the case for MQXFA components, but should be checked during flaw size analysis.

### *4.4.5 Crack propagation and arrest*

GradeCrack propagation requires a flaw of sufficient size in a specific location and orientation, with sufficient local (elastic) strain energy at the crack tip to continue propagation. In all all cases, design criteria for MQXFA assumes a probabilistic flaw in the least preferential location and orientation for assessment. Initiation processes are ignored and only stable crack growth criteria are assessed within elastic models. These are provided via Grade II or III analyses which may require iteration to assure elastic regime is achieved for this analysis.

Critical flaws that may propagate based on design criteria require further assessment. In these cases an iteration of the Grade III stress analysis is required with an included flaw of the size and geometry calculated in the initial Grade IV assessment to determine a new stress field at the crack tip for further Grade IV analysis. Iteration may be required to assure Saint-Venant's principles still hold within the sub-model, perhaps by increasing the volume of the sub-model if required.

Critical stress intensity may exist only near stress discontinuities. Propagation of a critical crack to regions of lower stress can truncate crack growth. Assuming a critical crack exists, it will likely self-arrest when growing into regions of lower stress. While less conservative than the conditions stipulating no stable crack growth, demonstrating that a potential crack will truncate is allowed. Further assessment of such a crack, and how it may impact the performance of the overall design is required. Consequences of such a failure in certain components may be small, allowing more to be accepted. For components where impact of failure may be large, more stringent design criteria or component rejection will be stipulated, or may lead to Re-Design of Component.

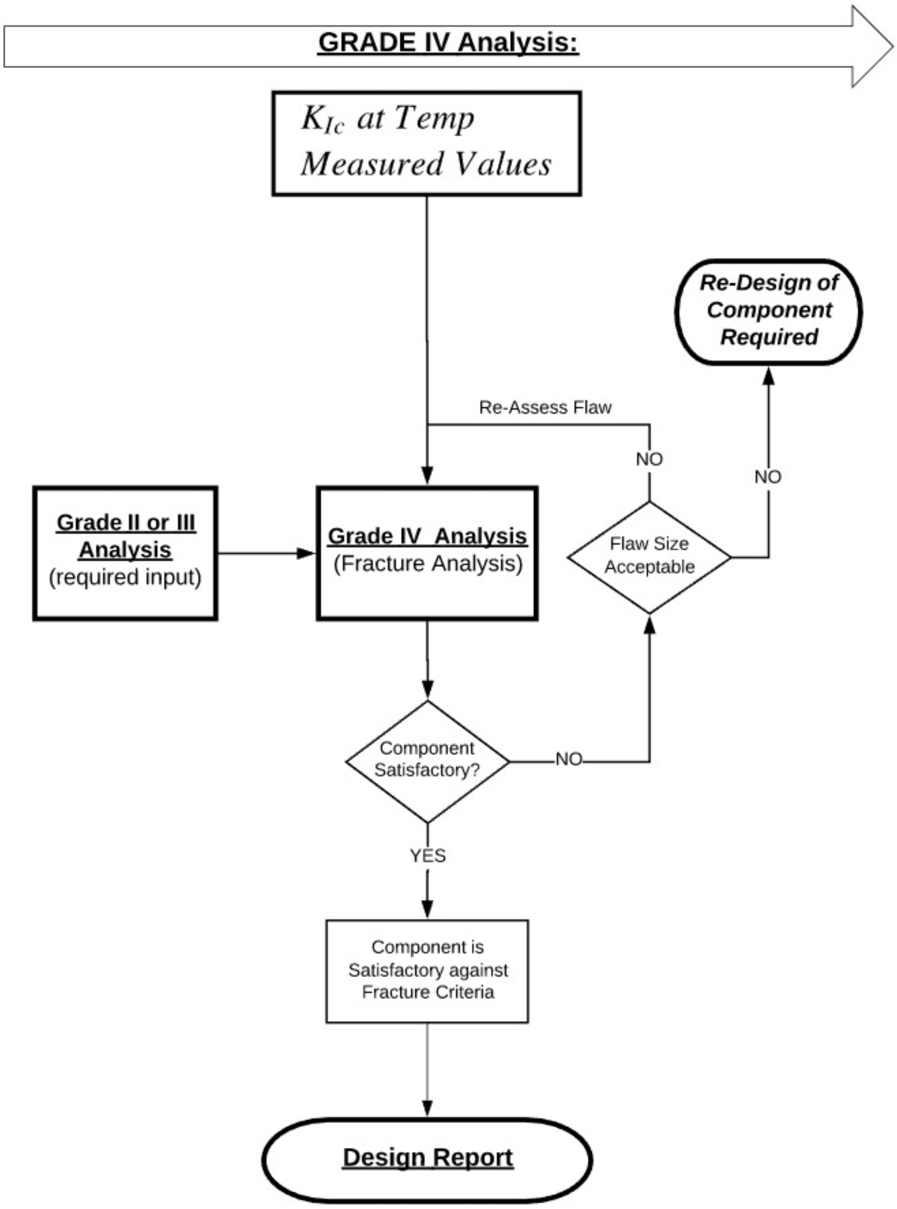


**Fig. 12:** Flowchart describing Grade IV Stress Analysis procedure.

# 5 Metallic Component Design Criteria

## 5.1 Scope

This section describes the design criteria for structural components of MQXFA. This specifically includes all components of the MQXFA magnet structure that are used to load and then maintain the preload on the superconducting quadrupole coils of MQXFA. This document does not include the welded pressure vessels of the LHe containment vessel or cryostat. The LHe containment vessel and cryostat will follow the B&PVC Section II & III [3], and the PED [5] for eventual use at CERN. The MQXFA magnet structures are completely inside of the LHe containment vessel.

Many of the materials used in the MQXFA structures are considered 'brittle' and perhaps unsuitable for use in pressure vessels as described in various standards. The Aluminum alloys used are not generally weldable, and the pure iron required for magnetic properties are similarly brittle. Other materials used, e.g. various Stainless Steels, while accepted in the B&PVC [3] will be treated similarly here as brittle if $K_{Ic} \leq 100\ MPa\sqrt{m}$, with appropriate material properties used for assessment.

## 5.2 Static Stress Limits

The static stress limit of any component represents a catastrophic failure of the component; limiting its ability to provide requisite loads to the structural assembly. The static stress limits are governed by either Plastic Collapse, or Fast Fracture. Plastic collapse occurs when the the primary stresses reach the plastic limit across a significant section of a given component, forming a plastic hinge, which limits the load capacity of the component. Fast Fracture may occur when the local stress intensity exceeds a critical value allowing a crack to propagate catastrophically through the section of the component. Intermediate values of failure between plastic collapse and fast fracture may exist where the component no longer provides the requisite load capacity. These design criteria are aimed to prevent either case.

The static stress limits are based on material properties measured by the MQXFA project, its previous research program (LARP), or reported in available literature.. They are all from uniaxial tensile tests at relevant temperatures as available. It is well established that 'serrated yielding' occurs above the 0.2% strain yield criterion at cryogenic temperatures–see ITER Design Criteria Section MC 3.2 [1]. For the purposes of this document the onset of yield at the 0.2% offset will be used as an assessment criteria at cryogenic temperature unless relevant data is available to calculate the flow stress, $\sigma_c$. Enhancement or degradation of moudulus, flow stress, and critical stress intensity values at cryogenic temperatures will be included as supported by test data.

The design criteria presented in this document for MQXFA components approach the static stress limits typically defined in the B&PVC [3], for plastic collapse. Load Factors for Fast Fracture are taken from FFS-1 [4]. The formulation of safety factors defined in the B&PVC [3] typically limit primary stresses $(\sigma_m + \sigma_b)$ to either 2/3 $\sigma_y$, or 1/3 $\sigma_u$ [3] (section II, section D, Appendix 2) and are based on the formation of a 'plastic hinge' through the net section. The conservatism presented in the code predates extensive use of Finite Element Modeling. Assessment criteria for MQXFA will assess peak equivalent stress, $\sigma_v$ (von Mises stress), against the yield stress $\sigma_y$, and max principal stress, $\sigma_p$ against fast fracture, as reported from stress models available from the graded analysis approach. This document uses yield stress $\sigma_y$ for plastic collapse and $K_{Ic}$ properties for fast fracture (at relevant temperatures) for assessment, and will use recently developed failure assessment diagrams (FAD) [6], [4] to include the full range of static failure mechanisms. While the use of FAD have not been normalized in the B&PVC [3], they are specifically used in ASME FFS-1 [4], and are used here.

### *5.2.1 Limiting Stress Values*

For structural components in MQXFA, values of the "Limiting Stress" or "Stress Intensity" are material and temperature dependent. They are the limiting values against plastic collapse and fast fracture against which failure criteria are assessed, and margins to failure or factors of safety are reported. The temperature range considered is 4K to 300K.

For structural materials, including bolts, the limiting Stress, $S_m$ value is defined as 0.8 $\sigma_y$, for purposes of assessing plastic collapse against von Mises stress, $\sigma_v$, and 0.8 $\sigma_c$ for assessing fast fracture. See section 3.1.5 for notes on appropriate use of $\sigma_c$. The factor of 0.8 is used to account for data uncertainty after inclusion of relavent safety factors.

### *5.2.2 Distortion energy limits for Peak Stress*

The von Mises stress will be calculated from the analysis results presented in section 4. Based on elastic stress analysis, with limited plasticity, the following stress limits shall be met:

- Membrane stress shall not exceed $1.0\ K\ S_m$

  [Ref. [3]] Section III, NB-3221.1]

- Local Primary stress shall not exceed $1.25\ K\ S_m$

  [Ref. [3]] Section III, NB-3221.2]

- The multiplier $K$ is dependent on level of service conditions presented next.

Case 2 is modified from the cited reference, which has a multiplier of 1.5 versus the 1.25 shown above. In the codes, $S_m$ is 2/3 $\sigma_y)$ with the 1.5 factor making the allowable stress limit above equal to $\sigma_y$. The factor of 1.25 is used here as $S_m = 0.8\sigma_y$, so that in this case as well, the result is $\sigma_y$.

In cases where peak stress locally exceeds $\sigma_y$, an elasto-plastic analysis described in section 4.3 is required to allow the Membrane and Bending components to be extracted for comparison to these Figures of Merit. Most designs in MQXFA will not approach these limits as the designs are typically assessed against peak loads to limit the size of plastic regions, this will typically hold the Primary Stress to well within the allowable.

### *5.2.3 K-Factors*

The appropriate K values for various load conditions are:

- For Normal operating conditions, $K = 1$

  [Ref. [3]] Section III, NB-3222]

- For Anticipated conditions, $K = 1.1$

  [Ref. [3]] Section III, NB-3223]

- For Unlikely conditions, $K = 1.2$

  [Ref. [3]] Section III, NB-3224]

- For Extremely Unlikely conditions, $K = 1.35$

  [Ref. [3]] Section III, NB-3226]

While the loads calculated using the above $k$ for unlikely events can yield allowable stresses above yield, they are assessed against the membrane or primary load, not the peak stress.

| Damage Limits and Recovery from Events | | | |
|---|---|---|---|
| Condition | Probability | Damage Limit to Component | Recovery from Damage |
| Normal (A) | $P = 1$ | The component should maintain specified service function | Within specified service limit, anticipated maintenance, and minor adjustment |
| Anticipated (B) | $10^{-2} \leq P \leq 1$ | The component must withstand this loading without significant damage requiring repair | Within specified operational limit, anticipated maintenance, and minor adjustment |
| Unlikely (C) | $10^{-4} \leq P \leq 10^{-2}$ | Local Material plasticity, or insulation failure which may necessitate removal of component for repair, replacement, or inspection | May require repair or replacement or re-work of magnet structures |
| Extremely Unlikely | $10^{-6} \leq P \leq 10^{-4}$ | Not Used | |

**Table 3:** Damage Limits and Recovery from Events [2]

, [1]

### 5.3 Fracture Assessment

The R6 method was developed for thick wall pressure vessels and piping at temperatures below which creep phenomena occur for the Nuclear industry in the UK in the mid-1970's. It has since been noted to be overly conservative in the cases of tough work hardening steels now typically used in the nuclear and chemical processing industries. It has been modified since to account for these effects, but the most basic version is quite valid for materials such as 7075-T6 which do not exhibit significant strain hardening. Bloom 1980 [16]. For the purposes of this document, only the flow stress, $\sigma_c$, will be used to account for the enhanced strength of these tougher stainless steels.

The R6 FAD (Failure Assessment Diagram), presented in fig. 3 in Section 4 above, and replicated in this section in fig. 13, captures failure by LEFM (elastic fracture), and plastic collapse simultaneously. This is the main benefit of the R6 approach, it captures the broad range of elastic fracture, ductile tearing, and plastic failure in a single plot. The envelope of the FAD is known to fall under the failure points of data for various materials for various load points in the units of the plot. The vertical axis is normalized to critical stress intensity $K_{Ic}$ for the crack geometry considered, and the horizontal axis is normalized to flow stress, $\sigma_c$, of the material assessed. Materials which exhibit significant strain hardening tend to extend beyond unity on the horizontal axis for load cases that map in that direction, an advantage requiring Elasto-Plastic Fracture Mechanics (EPFM), an approach that is not taken here.

The FAD curve, shown in eq. 4.1, is not developed mechanistically. It is simply a curve developed to fit under failure points and meet boundary conditions of unity on both axes of the FAD. Other curves for strain hardening materials are available in BS-7910 [7]. The R6 method plots assessment points, ($S'_r$, $K'_r$), in fig. 13, in units of the FAD, called the 'Load Point.' Load points inside of the FAD curve are safe from failure, load points falling outside or on the curve may fail–they require mitigation plans i.e. change of design/material/loading, or assessment of arrest.

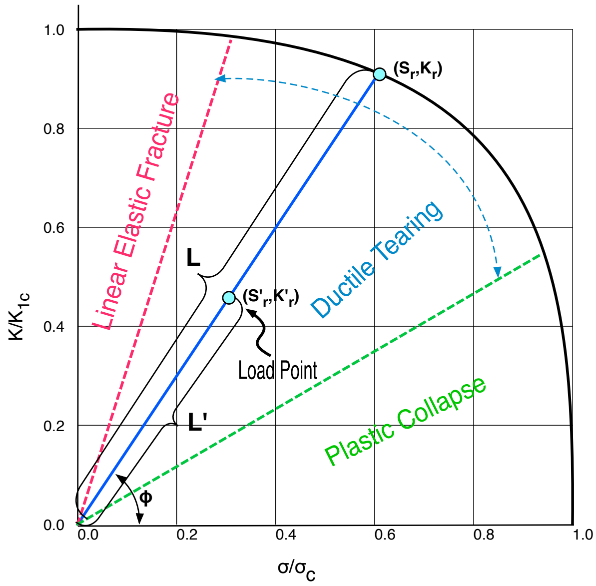


**Fig. 13:** Failure Assessment Diagram.

The "Projected Load Point," ($S_r$, $K_r$) can be determined using values from the "Load Point," and projecting them onto the $K_r(S_r)$ (FAD) curve using the following equations:

$$\phi = atan\left(\frac{K_r'}{S_r'}\right) \tag{5.1}$$

$$S_r = \frac{2}{\pi}\, acos\left(e^{\frac{(-\pi\ cot(\phi))^2}{8}}\right) \tag{5.2}$$

The equation for $\phi$, is simply the angle from horizontal of the line through the Load Point, ($S_r'$, $K_r'$). Eq. 5.2, for $S_r$ uses $\phi$ to project the line onto the FAD curve, solution provided in Bloom [16]. To determine $K_r$ from $S_r$, eq. 5.2 is evaluated in eq. 4.1 for the FAD. In units of $\phi$, plastic collapse dominates under 30°, and LEFM dominates above 70°–these lines are plotted in fig. 13. Failure in LEFM is dominated by $K_{Ic}$.

The magnitude ratio ($L/L'$), is a measure of the load margin for an object with a given flaw. This is called the "Load Factor" and should not be equated directly with "Factor of Safety," which is reserved for assessment against plastic failure criteria for the net section in an un-flawed structure. For the example shown in fig. 13, the load factor is 1.9. $K_r'$ in this formulation assumes a flaw of a particular size and geometry, described in Section 4.4, to assess against. $S_r'$, is similarly assessed at the location of the crack tip, which uses the cubic expansion of the peak principal stresses defined in eq. 4.6, however, for small flaw sizes, the un-flawed structure in fig. 13 would be assessed simply along the horizontal axis versus the flow stress under the same load conditions, the Factor of Safety against local yielding would be $\sim$ 3.3 i.e. $(1/S_r')$ – noting use of $\sigma_c$ versus $\sigma_y$ in the FAD.

The ordered sets, ($S_r'$, $K_r'$), and ($S_r$, $K_r$) are required to calculate the Load Margin:

$$Load\ Factor\ = \sqrt{\frac{(S_r\,^2 + K_r\,^2)}{(S_r'\,^2 + K_r'\,^2)}} \tag{5.3}$$

As the Load Factor approaches unity with increased flaw size, understanding potential flaw characterization and material properties becomes more critical. Flaws do not propagate along the load line

(L); the load line is only used to assess the Load Factor. A flaw is considered critical in size if its Load Factor is unity. Acceptable values of load factor are discussed in the next section.

### *5.3.1 Fracture Allowable Limits*

The stress intensity factor $K_I$, calculated in section 4.4, and the assessment criteria (Load Factor) is described here. The probabilistic load scenarios, A-C are described in table 3. Acceptable Load Factors for use on the FAD are described below, for example in table 4, a flaw with a load factor of 1.2 is deemed acceptable for Normal operations. Flaws which assess above this Load Factor, may require tighter inspection criteria to allow component acceptance.

| Operating Load Factor | |
|---|---|
| Normal (A) | 1.2 |
| Anticipated (B) | 1.1 |
| Unlikely (C) | 1.0 |

**Table 4:** Load Factors for use in Design

These are consistent with use of a material up to 0.8 $\sigma_y$ for Normal (A) loads. The $K_{Ic}$ values from test data are used to construct the FAD. As these test values are typically limited in sample size, the sample size does not yeild to normal statistics. The minimum of three equivalent approach is used to determine which values of the test results will be used. If test data is available in any of the other standards used here, e.g. Mil-HDBK-5 [8], their use is acceptable.

| Minimum of three equivalent (MOTE) | |
|---|---|
| Number of Fracture Tougness Results | MOTE Value |
| 3 to 5 | Lowest |
| 6 to 10 | Second Lowest |
| 11 to 15 | Third Lowest |

**Table 5:** Value from Test results to use using Minimum of Three Equivalent, BS 7910 [7] Section 7.1.5

The MOTE approach, while described and accepted in the standard, may not be the most conservative. More recent results investigating a characteristic statistical fit to limited sample size data may be more appropriate. For highly skewed data, or ones with low outliers, the lowest reported valid $K_{Ic}$ test result from E399 [10] Compact Test Specimens will be used.

# 6 Bolts and Keys criteria

For the purpose of MQXFA, there are no bolted flanges as found in pressure vessels or other structures. Some pre-load members, e.g. Tie-Rods providing axial compression to the magnet, may use joint separation as a criteria where the tension members would then take all of the externally applied loads; however the pre-load value is chosen to prevent this in all load cases. Similarly, keys and pins are not employed in the traditional sense to independently carry shear loads as applied to a bolted joint. Keys are used primarily for location purposes, though may see shear loads during eccentric primary loading of the structure at Room Temperature. Some keys will see significant compressive loading during cool down by design.

Pre-load stresses are often considered Secondary stresses, as they are strain based, not load controlled, e.g. pressure loads in a pressure vessel. The primary purpose of the MQXFA structure is to provide pre-loads to the magnetic coils, so all stresses induced by pre-load are considered primary.

Bolts, keys, and treaded tension members, can be designed for static limits based on average stresses across their section.

For pre-load at Room Temperature:

– Pre-load Stress shall not exceed $0.75\sigma_y$

– Pre-load shall be sufficient to prevent joint separation

For Loads at Cold and in Operation

– Pre-load Stress shall not exceed $0.75\sigma_y$

– Values for $\sigma_y$ at $4K$ shall be used.

It should be noted, that the material selection for tension members is selected specifically to increase in tension upon cool-down, and their strength is typically enhanced at $4K$.

# 7 Reports

The end result of all analysis shall be an engineering note. This note can include multiple components if appropriate, for example the stresses are result of an analysis of an assembly with sufficent margin on all components. Generally analysis Grades 3 and 4, or where mitigating actions change the base design, an engineering note will be required for unique components.

## 7.1 Design Data

The report will list all relevent design data including all material properties used and a reference for their origin. The loads applied to the components or assembly, and a reference to the drawings and or geometry used for input.

## 7.2 Graded Analysis

Referring to this document describe the grade of analysis employed, and description of transitions to higher grades if required be dscribed. Auxiliary equations or description of the analysis method should be kept brief but must include boundary conditions applied to FEM, element types and their inputs, if not included in Design Data above, so that they can be reviewed without requiring access to the FEM directly.

## 7.3 Assess Analysis

If any iteration is required in the design to mitigate stress concentrations, describe what actions were taken. This will be considered backup to any engineering change request if required.

#### 7.3.1 Apply Design Criteria

Referring to this document, cite the relevent criteria employed to satisfy the design

# Appendices

## A Influence Coefficients used in fracture analysis of MQXFA

Stress intensity varies strongly with $a/c$ ratios $\leq 1$ as shown in figures A.1 and A.2. It can be seen that the calculated $K_I$ for an embedded centered crack, figure A.1, is generally lower than that calculated for a crack of similar characteristic size at the edge of the structure. Figures A.1, and A.2 are plots of $K_I$ using only membrane stress, and normalized to stress in an un-flawed structure. They are for a finite width and thickness member with $a/t = 0.1$ and $W/c > 20$. These conditions assure validity of the calculation. Values would change for other ratios, but the trends used here remain similar and are consistent with typical component geometries used in MQXFA. It should be mentioned that $c$, the crack width, should be $<<$ than the component width for the assumptions of a semi-elliptic crack to remain valid. If $c$ approaches the component width, a different set of influence coefficients are required, for instance in thin lamina, where width is much less than thickness.

### A.1 Flaw Shape Characterization

Proper selection of an appropriate assessment ratio for $a/c$ is important. Where $K_I$ for the $\phi = \frac{\pi}{2}$ direction is in the $a$ direction, and $\phi = 0$ direction is along $c$, for a given flaw size, and either $a$, or $c$, is the maximal characteristic flaw size, figure A.1 shows that an embedded elliptical flaw may grow in either direction (if a critical stress intensity value is exceeded) until $a = c$, i.e. until the flaw is circular ($a/c = 1$). However, for an edge-cracked geometry, shown in figure A.2, at $a/c = 1$, the calculated $K_I$ in the $\phi = \frac{\pi}{2}$ direction exceeds the $a$ direction by 10-15%. It is likely then, that an edge crack, if allowed to grow, will grow in the 'c' direction until ($a/c = 0.8$), therefore use of the influence coefficients for ($a/c = 1$) in the $\phi = 0$ direction is appropriate. The change in calculated $K_I$ is only some few percent, thus within typical load margins.

It should be noted that these values are to be used for design assessment, are tied to inspection limits, and that crack growth in the $a$ direction (through thickness), is the critical direction. Setting the inspection limit to under the critical flaw size should render flaw geometry irrelevant of detected flaws for the purpose of design criteria, i.e. flaw orientation and geometry is unimportant, if the characteristic dimension is sub-critical, and use of Influence Coefficients with $a/c = 1$ and $\phi = 0$ are conservative, as a flaw of any detectable size below critical will equilibrate at sizes that remain below critical.

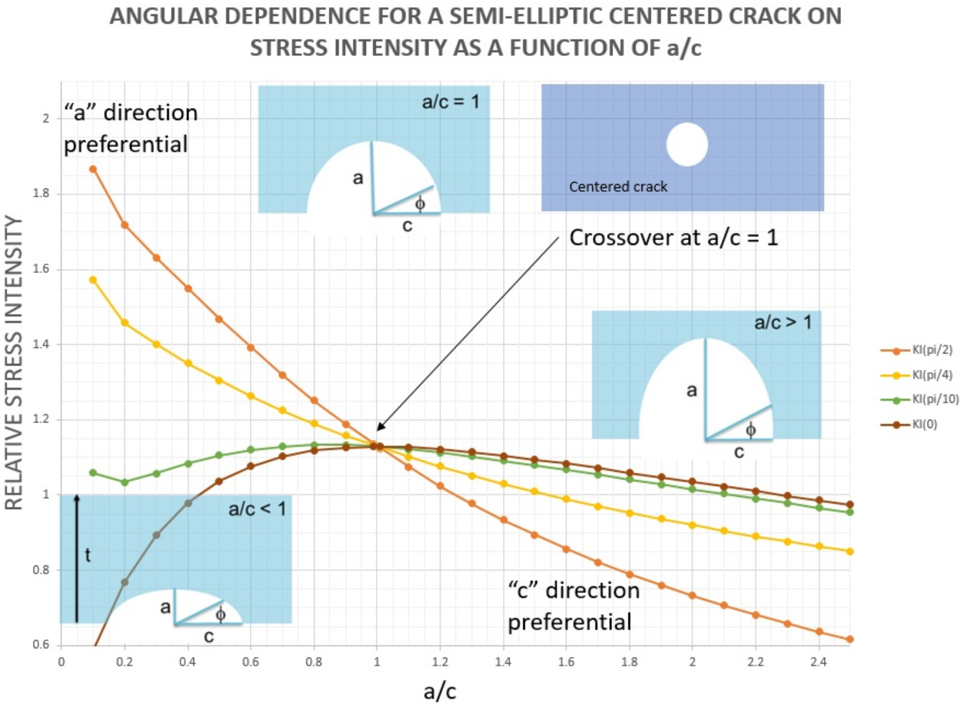


**Fig. A.1:** Plot of Stress Intensity for semi-elliptic flaw centered on the cross-section subject to membrane stress

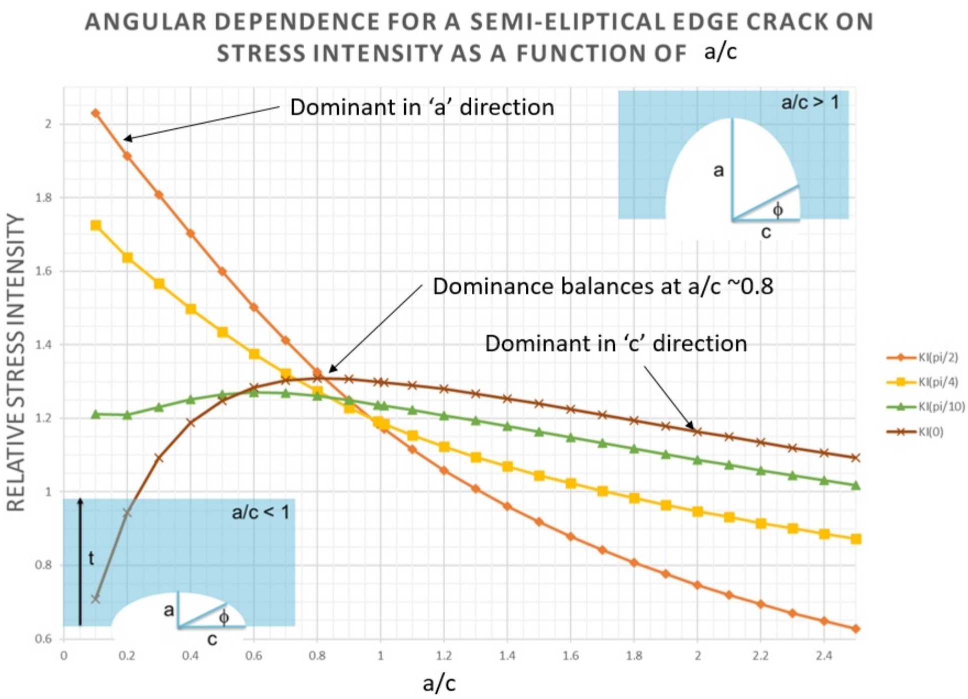


**Fig. A.2:** Plot of Stress Intensity for semi-elliptic flaw at the edge of the cross-section subject to membrane stress

### A.2 Influence Coefficients and Equations used in Calculations

The influence coefficients, $G_i$ described in section 4.4, are often only tabulated for a few relative crack length ratios, $(a/t)$, e.g. 20, 50, and 80% through thickness. They vary slowly with $a/t$ ratio with slight non-linear behavior. Most flaw sizes of interest are much smaller than 20% through thickness, so projecting the $G_i$ to smaller $a/t$ ratios requires a quadratic fit to the 3 reported values in available tables.

An example fit to data points for a semi-elliptic part-through flaw with a ratio of $a/c = 1$, in the $\phi = 0$, '$c$' direction is shown for a cantilevered plate in fig. A.3 for reference.

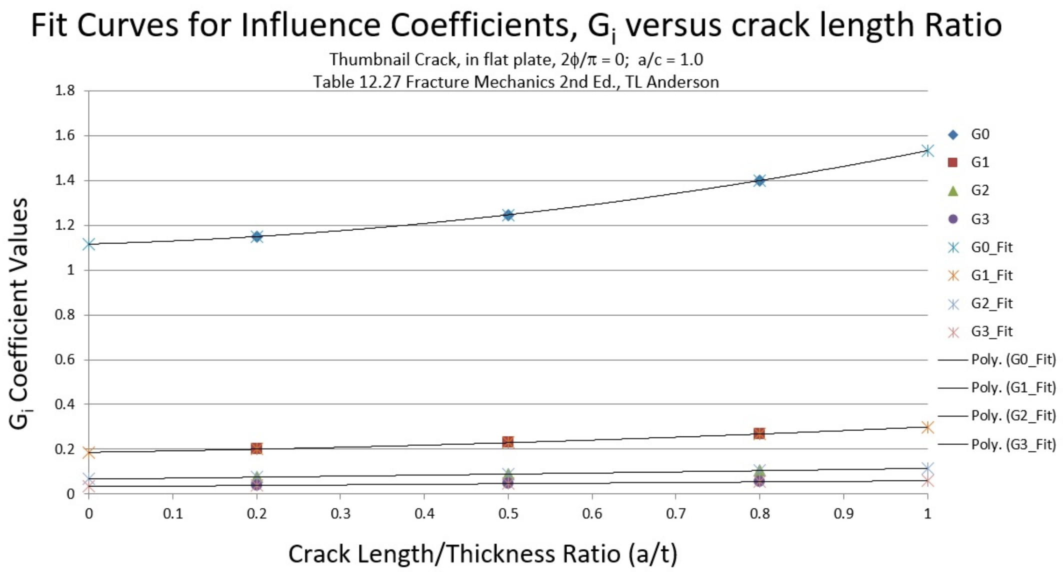


**Fig. A.3:** Plot of $G_i$ for semi-elliptic flaw at the edge of Cantilever Plate subject to a cubic fit of the through section stress profile; values for curve fits taken from Anderson [14].

Figure A.2 shows that the calculated $K_I$ for $\phi = 0$ $(c)$ are $\sim 10\%$ higher than the $\phi = \pi/2$ $(a)$ direction. Figure A.3 shows that the $G_i$ decrease monotonically with decreasing $a/t$ ratio, and the value at $a/t = 0$ is ∼3% less than the value for $a/t = 0.2$. While this expansion method is useful to study flaws which may propagate to values larger than $a/t = 0.2$, for flaw sizes under $a/t = 0.2$, use of the influence coefficients for $a/t = 0.2$ are generally conservative. Figure A.3 also illustrates that summed enhancement to calculated $K_I$ from bending and higher order contributions to peak stress are limited to diminishing modifiers of $\sim 25\%$ at $a/t = 0$ compared to that due to the membrane stress, $G_0 A_0$ from equation 4.9. Higher order terms in equation 4.9 from equation 4.8

| $G_i$ for $a/c = 1$, $\phi = 0$ | | | |
|---|---|---|---|
| $\frac{a}{t}$: | 0.2 | 0.5 | 0.8 |
| $G_0$ | 1.150 | 1.247 | 1.400 |
| $G_1$ | 0.200 | 0.229 | 0.268 |
| $G_2$ | 0.075 | 0.089 | 0.104 |
| $G_3$ | 0.038 | 0.046 | 0.054 |

**Table A.1:** Influence Coefficients for semi-elliptic surface crack in a flat plate

Comparing the $G_i$ from table A.1 to those in tables A.2 and A.3, that are for a thick walled cylinder with $t/R_i = 0.10$, which is relevant to the aluminum shells of MQXFA, it is seen that the $G_i$ for the cylinder differ only slightly from those of the flat plate. They are $\sim 1\%$ higher for the outside crack, versus $\sim 1\%$ lower for the internal crack compared to the flat plate. For completeness, the $G_i$ for cylinders will be used for shell analyses.

Most components of MQXFA can be approximated using the influence coefficients described here, however some components, e.g. the 'Axial Rods' and 'Tie Rods' are solid cylinders subject mostly to tension forces and in few cases limited bending. For these, the $K_I$ solution is taken from the Damage Tolerant Design Handbook [9]. The geometry is shown in figure A.4.

| $G_i$ for $a/c = 1$, $\phi = 0$ | | | |
|---|---|---|---|
| $\frac{a}{t}$: | 0.2 | 0.5 | 0.8 |
| $G_0$ | 1.140 | 1.219 | 1.348 |
| $G_1$ | 0.197 | 0.221 | 0.255 |
| $G_2$ | 0.074 | 0.085 | 0.099 |
| $G_3$ | 0.038 | 0.044 | 0.051 |

**Table A.2:** Influence Coefficients for semi-elliptic surface crack on the inside of a cylinder with $t/R_i = 0.10$

| $G_i$ for $a/c = 1$, $\phi = 0$ | | | |
|---|---|---|---|
| $\frac{a}{t}$: | 0.2 | 0.5 | 0.8 |
| $G_0$ | 1.156 | 1.266 | 1.453 |
| $G_1$ | 0.202 | 0.236 | 0.286 |
| $G_2$ | 0.076 | 0.092 | 0.113 |
| $G_3$ | 0.039 | 0.048 | 0.059 |

**Table A.3:** Influence Coefficients for semi-elliptic surface crack on the outside of a cylinder with $t/R_i = 0.10$

| Description | Illustration | References |
|---|---|---|
| Surface Crack in a Solid Cylinder | 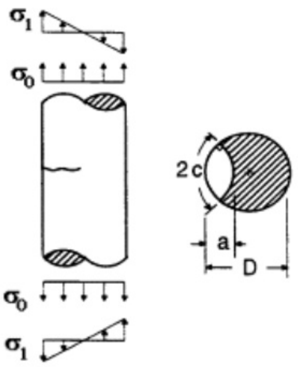 | Forman & Shivakumar [1986]<br>Forman, et al. [1998] |

**Fig. A.4:** Geometry for a surface crack in a solid cylinder subject to tension and bending loads.

$$K_I = (F_0\,\sigma_0 + F_1\,\sigma_1)\,\sqrt{\pi a} \tag{A.1}$$

Where $\sigma_0$ and $\sigma_1$ are the membrane and bending stresses. For appreciable flaw sizes, these stresses need to adjust for the decreased net-section and eccentricity of the remaining section. Most cylindrical members in MQXFA are Stainless Steel with $K_{Ic} > 100\ MPa\ \sqrt{m}$, so critical flaw sizes may be large. After an initial calculation of critical flaw size using just the membrane stress, an FEM with included flaw that reports $\sigma_m$ and $\sigma_b$ should be used with the full calculation including the bending term $F_1$. Iteration may be required to determine actual critical flaw size, or one can choose to reject components with the initially detected flaw approaching this dimension. Detection limits should be set for this, and load margins determined for their acceptance.

The full equations for tension and bending follow:

$$F_0 = G\,[0.752 + 1.286\,\beta + 0.37\,Y^3] \tag{A.2}$$

And

$$F_1 = G\,[0.923 + 0.199\,Y^4] \tag{A.3}$$

$$G = 0.92\left(\frac{2}{\pi}\right) sec\,(\beta)\sqrt{\frac{tan\,\beta}{\beta}} \tag{A.4}$$

Where $Y$, and $\beta$ are:

$$Y = 1 - sin(\beta) \quad ; \quad \beta = \left(\frac{\pi}{2}\right)\left(\frac{a}{D}\right) \tag{A.5}$$

## B Initial Flaw Size Estimation

Components used in MQXFA with material properties that are considered brittle, e.g. $K_{Ic} \leq 100\ MPa\sqrt{m}$ will require inspection. Some components that require forgings, require as part of delivery an inspection report prior to further machining. Others may be inspected after final processing and can only be assessed afterward.As shown in Appenix A, flaws may grow from a characteristic size, to either ratios of $a/c = 1$ or $a/c = 0.8$ upon initial loading, but may still remain sub-critical afterward. To be clear, this assumption of growth is only for assessment purposes, as flaws that are sub-critical should not grow.

For Ultrasonic detection methods, detected flaws are proportional to area, not geometry. Detection limits for ultrasonic methods in wrought aluminum (and most other standards) are calibrated to circular flaws based on grade, described in ASTM B594 [11]. Nothing is said in the standard regarding minimal detection limit or resolution; it is assumed that the calibrated flaw size represents the 95% Confidence Limit of detection.

For the purpose of tying inspection results to the least favorable geometry, use of $a/c$ ratios with the highest stress intensity are used. To remain well within regions of validity, a ratio of $a/c = 0.2$ is used for an edge crack which has large enhancement in the $a$ direction as seen in fig. A.2. The area of an elliptic flaw is $A = \pi ac$. For circular calibrated flaws, the area is $A = \pi(D/2)^2$, where $D$ is defined as the detection limit for the various inspection grades. For a flaw with $a/c = 0.2$, i.e. $c = 5a$ the area is:

$$A = \pi ac = \pi 5a^2 = \pi\left(\frac{D}{2}\right)^2 \tag{B.1}$$

$$a = \frac{D}{2\sqrt{5}}\ ;\ 2c = \frac{5\ D}{\sqrt{5}} = D\sqrt{5} \tag{B.2}$$

A detected flaw with this geometry will start with a characteristic length of $a$, with $2c = 10a$ as illustrated in fig. B.1. Reducing above, the inspection limit $D$ for a given grade of inspection can yield a flaw with a width of $2.24\ D$, which may propagate in the $a$ (thickness) direction until it reaches an $a/c$ ratio of 0.8, to 1.0, here we choose a ratio of $a/c = 1$ for simplicity. Calibration flaws for given inspection class is shown in table B.1.

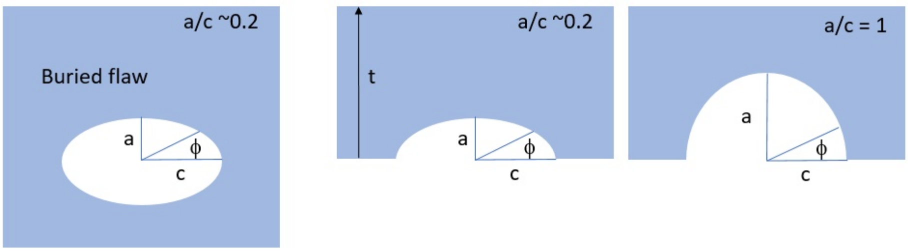


**Fig. B.1:** A flaw with area equivalent to the minimum detectable area, with least preferential orientation

It is important to note that the values in table B.1 are related to an initial scan of an as-yet unloaded component. The detectable flaws are smaller in the '$a$' dimension than what they may grow to, if critical, and that materials with given (required) inspection grades, showing flaws that are detected at these levels, will be rejected. The potential flaw size correlating to a given calibration size, is to be compared to the critical flaw size, and as this value is already 2.24X smaller than the inspection limit, the confidence level of finding flaws that would allow us to reject components is in excess of 99%, e.g. $> 4\sigma$ of a normal distribution ($2\sigma$ is the 95% Confidence Limit).

Table B.1 shows a range of detectable flaw sizes, e.g. if a critical flaw, assessed using Analysis in 4.4, and Criteria in 5.3.1 is 3 mm, an Inspection Class "A" will detect critical flaws, where if such a

| Inspection Class | Calibration Block | Allowable Critical Flaw Size |
|---|---|---|
| **AAA** | 0.40 mm | $>$ 0.90 mm |
| **AA** | 0.79 mm | $>$ 1.77 mm |
| **A** | 1.19 mm | $>$ 2.67 mm |
| **B** | 1.98 mm | $>$ 4.44 mm |

**Table B.1:** Flaw sizes correlated to Inspection Grades for Aluminum Forgings [11]

.

flaw is 2 mm, an Inspection Class of "AA" is required. Components which do not pass inspection will be rejected, or reserved for further qualification.

For other inspection methods, such as Dye Penetrant (LPT), or Magnetic Particle Testing (MPT), described in Appendix C, the size of any surface defect can be identified. As the characteristic shape and size of the internal flaw cannot be determined, any components with flaws detected in the region of peak stress will be rejected, unless the consequence of failure is low. Flaws found in other regions will be accepted.

## C Considerations in the inspection of materials

A number of techniques exist to inspect for flaws in materials in a non-destructive manner. The technique should be selected based on the properties of the material in consideration, and the critical flaw size that must be identified based on analysis and application of the design criteria above. The primary methods of inspection to consider are the following (but not exclusively, as other techniques exist that may be appropriate under some circumstances):

– Magnetic Particle Testing (MPT). This technique is possible when dealing with ferromagnetic materials such as steel. The material is magnetized and ferrous particles, either dry or in wet suspension, is applied to the part. Surface flaws and subsurface discontinuities can be observed since leakage magnetic flux attracts the ferrous particles more heavily in those areas.

– Dye Penetrant Testing (LPT). This technique applies to surface flaws in non-porous materials, including metals and ceramics. A low-surface tension fluid (penetrant) is applied to the surface, and capillary action works to draw the fluid into surface flaws. Once excess penetrant is removed, a "developer" solution is applied that draws penetrant from flaws and makes the flaws visible.

– Eddy Current Testing (ECT). This technique is applicable to conducting materials, primarily metals. This technique uses electromagnetic induction to probe for defects. Typically an AC current is produced in a coil local to the material surface, resulting in induced currents in the component under investigation. Flaws, either on the surface or in the subsurface, act to disturb the current flow resulting in a noticeable change in the impedance of the system.

– Ultrasonic Inspection (UI). Applicable to a variety of materials, including metals and nonmetal homogeneous materials. A beam of acoustic energy, typically in the $1-25$ MHz frequency range, is shot into the material using a transducer (typically a piezoelectric element) and the reflected (or in some cases transmitted) energy is monitored with a receiver. Surface and subsurface flaws result in a change in the amount of energy received.

– Radiography Inspection (RI). Applicable to a variety of materials. The technique is based on a change in radiation absorption as a function of material density. The component is subjected to penetrating radiation (typically x-rays or gamma rays), and the unabsorbed radiation monitored with detectors. Flaws appear due to the change in absorbed radiation density.

# D Materials properties 692

**Table D.1:** Materials properties used in FEA

| Material | Young's Mod. [GPa] 300K | Young's Mod. [GPa] 4.2K | Ult. Str. [MPa] 300K | Ult. Str. [MPa] 4.2K | Yield Str. [MPa] 300K | Yield Str. [MPa] 4.2K | CTE |
|---|---|---|---|---|---|---|---|
| Al 7075 T6 | 68.94 | 77.2 [5] | 489 [2] | 674 [3] | 420 [2] | 555 [4] | 4.12E-3[6] |
| SS 316 L [2] | 198 | 208[8] | 579 [7] | 1404 [9] | 289 [7] | 375[10] | 2.97E-3 [8] |
| SS 304 | 197 | 208[11] | 579 [7] | 1404 [9] | 289 [7] | 375[10] | 2.97E-3 [11] |
| Ti 6Al 4V | 130 | 150[14] | 896[12] | 1622[13] | 827[12] | 1497 [13] | 1.74E-3 [15] |
| ARMCO steel | 207 [17] | 224 | 241[18] | 681[18] | 121[18] | - | 1.98E-3[19] |
| Nitronic 50 | 193[20] | - | 813[21] | - | 517[21] | - | 2.54E-3[22] |
| G11 (in plane of fiber) | 28 [23] | - | - | - | - | - | 2.4E-3 [23] |
| G11 (normal to fiber plane) | 7 | - | - | - | - | - | 7.06E-3 [23] |

[1] Metallic Materials and Elements for Aerospace Vehicles Structure (MMEAVS), Department of Defense Handbook, Version 5J. Page 3-368.
[2] MMEAVS, Department of Defense Handbook, Version 5J. Page 3-381, Table 3.7.6.0(e1).
[3] MMEAVS, Department of Defense Handbook, Version 5J. Page 3-390, Figure 3.7.6.1.1(c).
[4] MMEAVS, Department of Defense Handbook, Version 5J. Page 3-391, Figure 3.7.6.1.1(d).
[5] MMEAVS, Department of Defense Handbook, Version 5J. Page 3-394, Figure 3.7.6.1.4
[6] Cryogenic Materials Data Handbook, Air Force Materials Laboratory. Page A-7p
[7] Material Certificate of Test.
[8] NIST Cryopgenic database.
[9] MMEAVS, Department of Defense Handbook, Version 5J. Page 2-226, Figure 2.7.1.1.1(b)
[10] MMEAVS, Department of Defense Handbook, Version 5J. Page 2-225, Figure 2.7.1.1.1(a)
[11] NIST Cryopgenic database.
[12] MMEAVS, Department of Defense Handbook, Version 5J. Page 5-58
[13] MMEAVS, Department of Defense Handbook, Version 5J. Page 5-61
[14] MMEAVS, Department of Defense Handbook, Version 5J. Page 5-63
[15] Cryogenic Materials Data Handbook, Air Force Materials Laboratory. Page F-3p
[16] Low Temperature Mechanical Properties of Copper and Selected Copper Alloys, U.S. Department of Commerce. Page 121
[17] ARMCO Pure Iron Brochur, AK Steel International.
[18] Metallurgy ARMCO and MAGNETIL materials, CERN Engineering Report, EDMS 1744165
[19] Experimental Techniques for Low Temperature Measurements, Jack Ekin. P 176
[20] Matweb.com, http://www.matweb.com
[21] Certificate of test.
[22] Notronic 50 Technical data. http://www.specialtysteelsupply.com/brochure/nitronic-50-technical-data.pdf
[23] Experimental Techniques for Low Temperature Measurements, Jack Ekin.

## References


[1] ITER Structural Design Criteria for Magnet Components (SDC-MC).

[2] NSTX STRUCTURAL DESIGN CRITERIA, Rev. 0,8/01/03, I. ZATZ, EDITOR.

[3] ASME Boiler and Pressure Vessel Code, July 1992 (sections quoted in text)

[4] ASME Standards Collection - ASME API 579-1/ASME FFS-1 2016.

[5] The Pressure Equipment Directive (PED) (2014/68/EU)

[6] British Energy Generation Limited, "Assessment of the Integrity of Structures Containing Defects", R6 Revision 4, Amendment 7, April 2009.

[7] The British Standards Institute, Guide to methods for assessing the acceptability of flaws in metallic structures, BS 7910:2013

[8] The Metallic Materials Properties Development and Standardization (MMPDS), formerly MIL-HDBK-5J, DEPARTMENT OF DEFENSE HANDBOOK: METALLIC MATERIALS AND ELEMENTS FOR AEROSPACE VEHICLE STRUCTURES

[9] USAF Damage Tolerant Design Handbook: Guidelines for the analysis and Design of Damage Tolerant Aircraft Structures
`http://www.afgrow.net/applications/DTDHandbook/`url

[10] ASTM E399-05 "Standard Test Method for Plane-Strain Fracture Toughness of Metallic Materials" 2005.

[11] ASTM B594 "Standard Practice for Ultrasonic Inspection of Aluminum-Alloy Wrought Products" 2013

[12] "yielding in Steel Sheets Containing Slits", Journal of the Mechanics and Physics of Solids, 8, (1960): 100-108

[13] "The mathematical Theory of Equilibrium Cracks in Brittle Fracture", Advances in Applied Mechanics, Vol. VII, Academic Press, New York, 1962, pp 55-129.

[14] "Fracture Mechanics: Fundamentals and Applications–Second Edition" Anderson TL, (1995)

[15] "Plane Strain Fracture Toughness of Aluminum Alloys at Room and Subzero Temperatures" FG Nelson (1971) DOI:10.1520/STP26927S

[16] Bloom JM, "Prediction of ductile tearing of compact fracture specimens using the R-6 failure assessment Diagram" International Journal of Pressure Vessel and Piping, (1980) DOI:10.1016/0308-0161(80)90026-5

[17] "MQXFA Magnets Functional Requirements Specification", US-HiLumi-doc-36 1535430 v.1.0 LHC-MQXFA-ES-0001